Thermoreflectance imaging of percolation effects and dynamic resistance in indium tin oxide nanoparticle layers

R. Chavez,[1] S. Angst,[2] K. Maize,[1] A. Gondorf,[2] G. Schierning,[3] D. E. Wolf,[2] A. Lorke,[2] and A. Shakouri[1]
[1]*Department of Electrical Engineering, University of California, Santa Cruz 95064, USA*
[2]*Falcultcy of Physics, CeNIDE, University of Duisburg-Essen, Germany*
[3]*Facultcy of Electrical Engineering, CeNIDE, University of Duisburg-Essen, Germany*

(Received 9 February 2012; accepted 10 September 2012; published online 16 October 2012)

Thin films of indium tin oxide nanoparticles are studied using charge-coupled device thoermoreflectance. High resolution sub-micron thermal images confirm that percolation in current conduction induces strongly inhomogeneous heat loads on the thin film. We experimentally show that the inhomogeneous current densities induce thousands of "micro-hotspots" that can be 20% hotter than the average Joule heating in the thin film layer and show comparable behavior in a resistor network. In addition to the percolation induced "micro-hotspots," we report major hotspots, with non-Joule behavior, whose temperature response is greater than I^2. We demonstrate that a temperature dependent resistor can account for an effective exponent larger than 2. Finally, it is shown that while ambient molecules modify the thin film conductivity by at least 20%, current conduction and percolation effects remain largely unchanged, but such chemical reactions can be nonetheless detected with thermoreflectance. © *2012 American Institute of Physics*.
[http://dx.doi.org/10.1063/1.4757960]

INTRODUCTION

Highly tin-doped indium oxide, In_2O_3:Sn^{4+} (ITO), combines metallic electrical conductivity with optical transparency in the visible spectrum of light. These desirable properties make it one of the most important conducting oxides, characterized by a direct band gap of just above 3 eV and typically highly doped, making it a degenerate semiconductor. ITO is widely used in flat panel displays and thin-film solar cell technology, light emitting devices, electrochromic devices, or heat-reflection coatings. ITO thin films are usually fabricated using physical vapor deposition methods such as evaporation of In_2O_3/SnO_2 powders or sputtering techniques that ensure good optical quality and high electrical conductivity, but these methods require expensive vacuum processes.

Alternative production routes for low cost applications are desirable. Printing techniques allow structuring without any subtractive wet chemical etching steps, as well as the use of flexible and temperature sensitive substrates, with obvious additional benefit for the market. Therefore, tailored ITO nanoparticles[1–3] are being synthesized and used for dispersions and inks.[4–6] Wet deposition techniques like ink-jet printing have been successfully applied[7–9] and have been tested for electronic applications. Typically, the nanoparticulate layers have to be optimized by an annealing procedure after deposition. Then, specific conductivities of 10^2–10^3 Ω^{-1} cm^{-1} (Refs. 4 and 10–14) can be achieved. Given the developments in the production and deposition of such a promising material, devices that actually use these recent developments seem to be further away that one would expect.

One reason for the delay in introducing ITO nanoparticles thin layers to the market can be found in the difficulties that go along with the development of the printing techniques and layer formation, especially if dispersions of nanoparticles are used as inks. The "coffee ring" effect makes it challenging to deposit homogeneous layers of nanoparticles. By applying a subsequent drying and annealing procedure, the formation of cracks has to be suppressed. In the case of ITO, sintering of the nanoparticulate thin films does not reduce the porosity of the films up to high temperatures,[4,13] as a consequence of a sophisticated coalescence mechanism of the oxide nanoparticles.[15] This means that the nanoparticle character of the film will always be preserved. Camouflaged by these technological challenges, another fundamental aspect has not yet been accounted for: nanoparticulate layers do not transport electrical current homogeneously; the current percolates through the film. As a consequence, the Ohmic heat will be deposited inhomogeneously with direct back coupling on the device. Inhomogeneous heating due to percolation effects becomes critical as high performance transparent films (transparency $\geq 90\%$ and $R_{Sheet} \leq 100$ Ω/sq) are most likely to fall in the percolative regime,[17] and therefore suffer from inhomogeneous heat loads.

Hence, it is the aim of this paper to study the inhomogeneous heat loads by experimental micro-scale thermal images and a simulation using an advanced resistor network model. Using thermoreflectance, we obtain the two dimensional Joule heating response in the thin film, which makes it possible to confirm inhomogeneities in the current patterns near the surface as well as the occurrence of unexpected non-Joule hotspots. Additionally, the stability of the granular ITO thin films under electrical load against ambient conditions was investigated, as reactions on the surface can significantly release or remove electrons from the conduction band[16] inducing a dynamic resistance that can change up to 10%–15% in a period of 2 h. With the aid of thermoreflectance, it is possible to

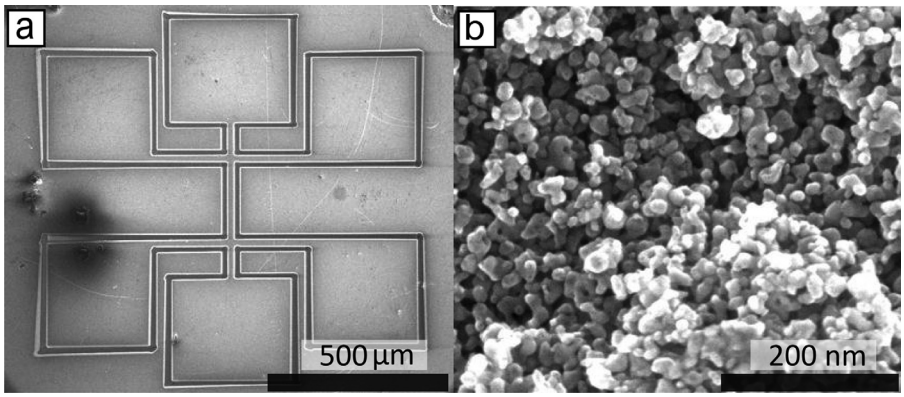

FIG. 1. SEM images show (a) the geometry used in the experiments and (b) the nanoparticle nature of the thin layer.

study how such chemical reactions modify current conduction paths.

EXPERIMENTAL METHODS

Sample preparation

We study granular layers shown in Figure 1, which have been obtained by printing stable dispersions of ITO nanoparticles onto glass substrates. The dispersions were processed by Evonik Industries AG. The particles were fabricated in a liquid co-precipitation process, and the mean particle size was in the range of 15–20 nm. The final thickness of the granular films was 800–950 nm. An advantage to this novel material is that these films can in principle be realized without the use of vacuum techniques and high temperature processes and can be patterned using inexpensive printing techniques. Electrical contact was made with tungsten microprobes with 100 μm tips.

CCD-based thermoreflectance measurement

Charged couple device (CCD) based thermoreflectance is a non invasive thermography technique used for high resolution thermal profiling of electronic and optoelectronic devices at the micro-scale. CCD based thermoreflectance or simply thermoreflectance—for the purpose of this article—has been shown to be a powerful tool in device characterization, performance, and reliability, as the high resolution thermal images unveil thermal distributions and in many cases hot spots. With shown spatial and thermal resolution of 250 nm and 10 mK,[18] CCD based thermoreflectance has been used to study heat loads and failure on solar cells,[19] transistors,[20] and thin films;[22] and in this article, we show its application towards the study of highly transparent nanoparticle layer to experimentally study percolation effects.

Thermoreflectance is based on the temperature dependence of reflectivity; by measuring the relative change in reflectivity of the surface of interest, the corresponding change in temperature can be inferred by the first order approximation that relates the relative change in reflectivity with a change in temperature[19]

$$\frac{\Delta R}{R_0} = \left(\frac{1}{R}\frac{\partial R}{\partial T}\right)\Delta T = C_{TR}\Delta T, \tag{1}$$

where the thermal induced change in reflectivity ΔR is normalized by the room temperature reflectivity R_0, and scaled by the thermoreflectance coefficient C_{TR}, which is wavelength and material dependent.[19]

To study the two-dimensional current paths and percolation effects near the surface of the ITO thin film, the Joule heating response was obtained using frequency domain techniques because they are known to be more robust to noise than transient techniques.[21] Hence, a homodyne setup supplying a sinusoidal signal to the DUT (device under test) under continuous 780 nm wavelength illumination was used. This specific wavelength was experimentally found to yield the highest thermoreflectance coefficient C_{TR}, in a calibration procedure that consists of heating the sample to a known ΔT under continuous wave illumination with 780 nm light, and recording the temperature induced change in reflectivity $\Delta R/R_0$ solving Eq. (1) for C_{TR}.

The frequency domain thermoreflectance technique used in our experiments supplies the DUT with a bi-polar, sinusoidal voltage signal with frequency f. As a consequence, within the reflective field, the Joule heating term becomes evident in the second harmonic producing an oscillating field with frequency $2f$ while Peltier effects are evident in the first harmonic at f. We can then write the surface reflectivity of the DUT as[23]

$$R(x,y,t) = R_0(x,y) + R_1\cos(2\pi ft + \varphi(x,y)) + R_2\cos(4\pi ft + \gamma(x,y)), \tag{2}$$

where R_0 corresponds to the DC reflectivity while R_1 and R_2 are proportional to the Peltier and Joule effects, respectively. The phase shifts φ and γ correspond to the observed thermal inertias associated with Peltier and Joule effects, respectively. It is shown in detail in Ref. 23 that when the reflectivity $R(x,y,t)$ in the form of an optical signal is oversampled by a factor of 8 at $8f$, R_0 and R_2 can be extracted from the 8 camera frames solving Eq. (1) for ΔT by replacing ΔR with R_2.

In order to study the electrical properties in parallel with the thermal response to see if current paths are modified by an ambient induced resistivity change, 4-wire resistance measurements were incorporated to the thermoreflectance LabView interface in order to monitor the resistance throughout the image acquisition process. This makes it possible to see the effect that a change in conductivity has on current conduction patterns in the nanoparticle based thin films.

Simulation details

We have simulated a two-dimensional resistor network on a square lattice well above the percolation threshold. The lattice sites are occupied up to a given density 1-p, where p is the porosity. Occupied sites account for ITO particles and each bond represents a resistor, which includes the particles resistance as well as the interface resistance. For the current purpose, it is sufficient to choose all resistances to be equal. Besides Joule heating, heat conductance according to Fourier's law is also taken into account. On each node, two dynamical variables are calculated, an electrostatic potential ϕ_i and a temperature T_i. The calculation depends on the following material parameters assumed to be constant: each node carries a specific heat, which is chosen to be equal for each particle, all bonds ij carry the same electrical conductance G and heat conductance Λ. The local potentials are calculated from Kirchhoff's laws, and the temperature at node i evolves in time according to

$$\dot{T}_i = \frac{1}{C_i}\left(\Lambda \sum_j \left[(T_j - T_i) + 0.5\dot{Q}_{ij}^J\right] + \Lambda_{sub}(T_{sub} - T_i)\right), \quad (3)$$

where the summation extends over the nearest neighbor nodes of i. Equation (3) includes a coupling of each particle i to the substrate, which acts as a heat bath with fixed temperature T_{sub} equal to the initial temperature. The heat $\dot{Q}_{ij} = G^{-1}I_{ij}^2$ produced at a contact is assumed to be delivered in equal parts to both particles. All material parameters are set to 1, except of the coupling to the substrate, which is $\Lambda_{sub} = 0.01$.

RESULTS AND DISCUSSION

Percolation effects, hot spots, and Joule heating

From the applications standpoint, it is of great value to know the degree of percolation within the granular layer because Joule heating will be deposited along the current paths. If an ITO nanoparticles electrode is to be combined with organic electronics, non uniform heat loads due to percolation effects of the current within the electrode will be present at the surface interface layer and may induce fatigue of the organic component and thus have fatal consequences for the device. The experimental, two-dimensional thermoreflectance images in Figures 2(b)–2(d) show the expected granulated Joule heating consequent from the inhomogeneous current densities. The granular heating is in the range of 5–8 μm in diameter, which would correspond to 500–800 nanoparticles and the highly porous system contributes to percolation and heat loads. The simulation of a two-dimensional resistor network with porosity $p = 0.39$ consisting of 250×50 lattice sites produces the steady state temperature distribution shown in Figure 2(e). While the spatial scale of the network is not arbitrary, is not necessarily in the same order as the experiment. Though the heat flow to the substrate as well as colder areas in the layer counteracts the strong local heating, a highly inhomogeneous temperature distribution is found in the steady state. The experimental temperatures are quantified in Figure 3 where temperature profiles are shown. The steady state local temperatures vary by about 20% around the average temperature in the channel. For some applications, a local temperature rise of this amount can already be considered as a hotspot. The reason for these temperature variations is illustrated by the network simulation, Figures 2(e) and 2(f). The current distribution within the nanoporous particle network is very inhomogeneous, but time independent, as the particle arrangement does not change. Therefore, there is an inhomogeneous, time independent pattern of Joule heat delivery. Heat conduction smears this pattern out, but not to the extent that the resulting temperature would be uniform throughout the sample. In the steady state, a pattern of temperature variations results, reflecting the spatial inhomogeneity of the current distribution. Of course, the

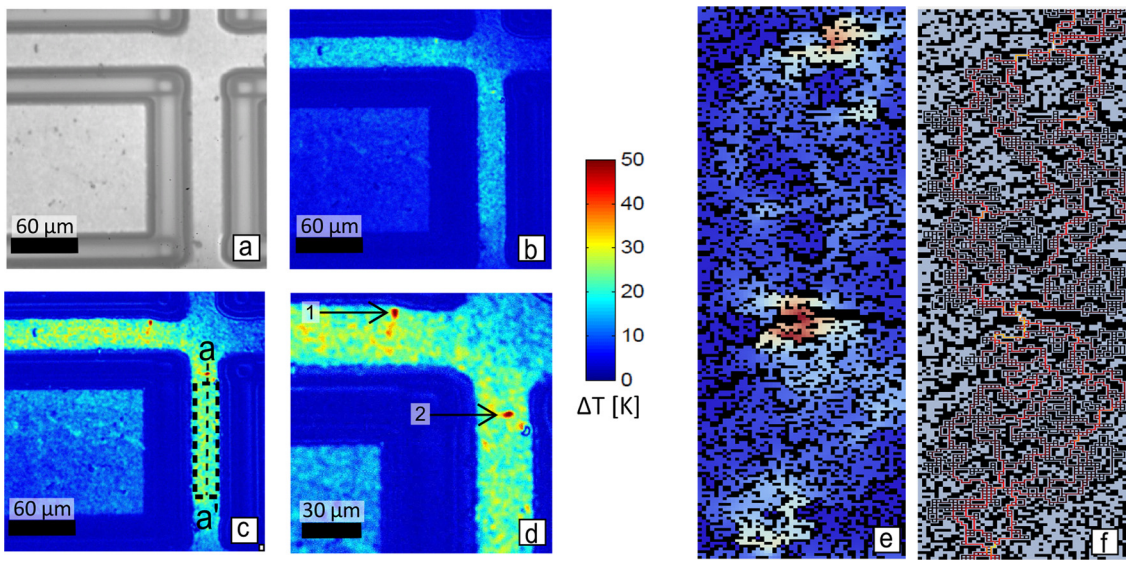

FIG. 2. (a) Optical image of the channel under investigation, (b) thermoreflectance image at 1.5 mA showing the granulated Joule heating. (c) Thermoreflectance image at 2.0 mA with the indicated profile and area used for temperature analysis. (d) Magnification from (c) shows the "enhanced hotspots." (e) A two dimensional simulated percolating network with arbitrary temperature units shows the inhomogeneous deposition of Joule heating, and (f) its respective current distribution.

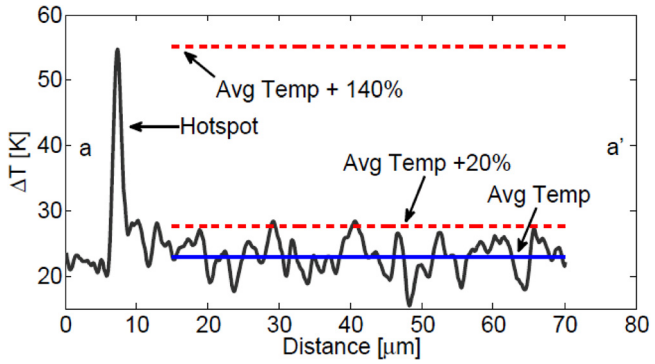

FIG. 3. Temperature profile along the path depicted in Figure 2(c) quantifies the variation in temperature along the sample. In blue, the average temperature of the channel (calculated from the enclosed area in Figure 2(c)) is used for reference. The hotspot is not used in the calculations.

amplitude of these temperature variations depends on the spatial resolution of the thermoreflectance measurement: averaging over the correlation length of the percolating network will essentially mask the temperature variation.

In contrast to the percolation-induced temperature variations, two major hotspots stand out in Figure 2(c), which are independent of the correlation length of the percolating network. At a total current $I_{tot} = 2$ mA, these hotspots reach a maximum ΔT of nearly 55 K, which is 140% above the average temperature in the channel as Figure 3 illustrates. In order to distinguish them from the percolation-induced hotspots, we call them "enhanced hotspots." This is justified by the following observation: the integrity of the thermal data has been checked by biasing the sample at different currents. One expects a quadratic response of Joule heating (ΔT) as a function of current

$$\Delta T \quad \alpha \quad P \quad \alpha \quad I^N, \tag{4}$$

with $N = 2$ under ideal resistive circumstances, P is the dissipated power, and I is the current.

In Figure 4(a), the exponent N is extracted for both the channel and the enhanced hotspots (dashed area in Figure 2(c) and hotspots labeled in Figure 2(d)). For the portion of the channel used for verification, $N = 2.03$. This is sufficiently close to 2 to confirm that the thermal images show Joule heating. This becomes crucial in validating the hotspots, for which $N = 2.38$. As seen from the optical image, there are no visible artifacts that could induce false temperature readings since the thermal image is a function of the optical image, this is important because surface features can induce false temperature readings. Even if the oxide surface had localized regions with different C_{TR} at the locations of the hotspots, the response should be nonetheless quadratic with current, yielding $N \sim 2$. Noise can also be ruled out, as the hotspots' temperature is calculated with a matrix's size that is 2 orders of magnitude smaller than the matrix used in the channel, yet the temperature response between the hotspots yields $N = 2.38$ for both hotspots. For a ΔT greater than 50 K, a temperature-dependent C_{TR} is a possibility and this could be the cause for the higher exponent N = 2.38. However as seen in Figure 4(a), in the extraction of the exponent N, only one point is in the range of $\Delta T \sim 50$ K. If this point were eliminated, the exponent of the hotspots would still be larger than that of the channel; therefore a temperature-dependent coefficient is not a concern.

Using the simulation ushered above, a Joule-like ($N = 2$) behavior for hotspots and colder particles is seen since the local current I_{ij}, which determines the temperature at sites i and j depends linearly on the total current flowing through the sample. However, taking into account temperature dependent resistance,

$$\rho(\Delta T) = a\Delta T + \rho_0, \tag{5}$$

where a is the coefficient of temperature dependent resistivity and ρ_0 the resistance at an initial temperature, the dependency of ΔT as a function of current changes dramatically. Let us consider a resistor $\rho(\Delta T)$ coupled to heat bath of constant temperature. In steady state, the Joule heating $\rho(\Delta T)I^2$ of the resistor is balanced by a heat flux $\Lambda\Delta T$ to the heat bath; and using Eq. (5), this results in

$$\Delta T = \frac{I^2\rho_0}{\Lambda - aI^2}. \tag{6}$$

For $I \ll \sqrt{\Lambda/a}$, Joule-like behavior $\Delta T \propto I^2$ occurs, but for $I \approx \sqrt{\Lambda/a}$, the temperature increases much stronger and diverges from Joule-like behavior (see Figure 4(b)). We

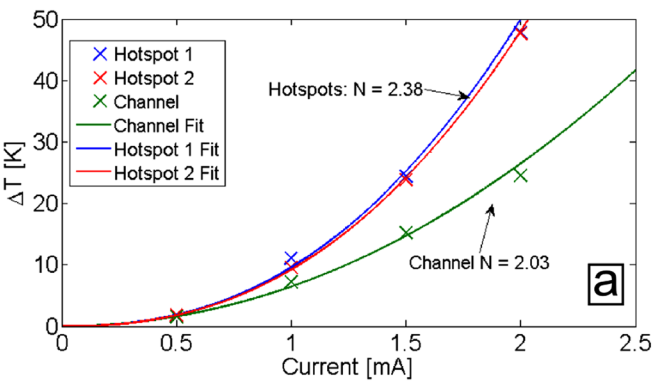

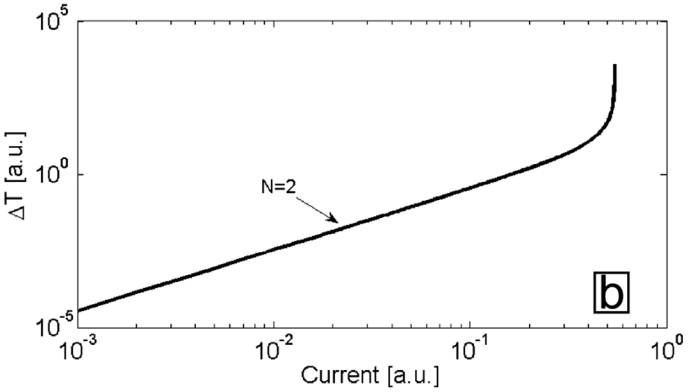

FIG. 4. (a) The experimental temperature response of the hotspots increases faster than the square of the current, with an exponent of 2.38. (b) The unexpected exponent can be explained by taking into account the temperature dependence resistivity of a percolating network where for low currents the effective exponent N = 2 and it diverges as a positive feedback loop is formed.

propose that the current flowing through an enhanced hotspot in the experimental sample is high enough to reach the regime characterized by non Joule behavior yielding an effective exponent $N_{eff} > 2$. From Eq. (5) and Figure 4(b), above a certain current, the current induced heating diverges from Joule like behavior and positive feedback is formed from the coupling of the temperature dependent resistivity and the dissipated power yielding exponents N greater than two. For non-Joule hotspots to appear in percolative networks, it is necessary that the positive feedback mechanism just mentioned is dominant over the negative feedback that would drive the current to find alternative pathways as the resistance increases at a given node. Moreover, if we take the diffusivity of polycrystalline ITO[26] and the frequency of the thermoreflectance measurement (0.625 Hz), the thermal diffusion length for the applied frequency on polycrystalline, non percolating ITO would be $\mu_p \sim 1 * 10^{-3}$ m^2, which is much larger than the enhanced hotspots' areas which are in the order of $5 * 10^{-12}$ m^2. This means that if we had a non percolating material, the enhanced hotspots would diffuse to a larger area. Therefore, the appearance of such enhanced hotspots seems to be only feasible in percolating networks.

The strongly inhomogeneous heating of the granular film, and furthermore the appearance of hotspots under electric load could have direct consequences on applications of printed ITO electrodes. This is of particular interest because the inhomogeneous heat load is a consequence of percolation effects, and as shown in Ref. 17 highly transparent films tend to be in the percolative regime, and hence subject to broad heat loads due to percolation effects. While difficult to extrapolate further, printing of nanoparticulate electrodes seems to be feasible only for electronic devices, which are highly tolerant to broad temperature regimes within the device.

Conduction patterns over time

It is known that ambient conditions can significantly modify conductivity when molecules in the air bind to the surface of the thin film removing electrons from the conduction band,[16] but until now, it had not been shown to what extent conduction patterns near the surface are modified by the chemical reactions since the reactions occur on the surface. To confirm the influence of ambient molecules on the macroscopic resistance, the sample chamber was evacuated and the resistance of the ITO nanoparticle layer measured over a period of 4 weeks and the results presented in Figure 5. Besides an increase of the resistance in the first 3 h, a monotonous decrease of the resistance can be seen and saturation is reached in the last 50 h of the experiment. The decreasing resistance can be explained by desorption of oxygen.[24] Comparable results have not been seen on compact ITO layers. The reason behind this is that TCO (transparent conducting oxides) layers usually have a thickness of above 100 nm to guarantee a reasonable conductance. Miyata *et al.* did some experiments on this field; they investigated the long term stability of several (TCOs) exposed to air with a high humidity. They found that if the film thickness is below 100 nm, the influence of ambient molecules becomes stronger with smaller scales.[25] Due to the porous structure of the nanoparticle layers, air can react with the ITO in the whole film. That is the reason why such a strong effect is noted even though our thin film is in the order of 1 μm.

To study how conduction patterns near the surface are modified by such chemical reactions in ambient conditions, 8 high resolution thermal images were taken in a period of 8.7 h and then mutually compared to see if the two dimensional Joule heating map is time variant. Since the goal is to monitor Joule heating for a period of more than 8 h, small shifts in the CCD image occur when imaging for such long periods of time at high magnification. Therefore, image shifting was corrected by reorienting the images with respect to surface features, this correction is necessary to make direct comparisons between images. Having verified that there is no shifting in the visual images, makes it possible to decouple variations in the thermal profiles from variations in the visual images. This means that a thermal profile pertains to the same physical region in all the images.

During the 8.7 h, eight thermal images were obtained. After the acquisition of each image, the sample was left in ambient conditions while resistance was recorded as illustrated in the time diagram in Figure 6(a). During the image acquisition time, the electrical measurements were halted. It can also be seen in Figure 6(a) that during the nearly 9 h experiment, the resistance increased by 24.8%, resulting in a power decrease of 19.9% because the voltage was held constant. Such a significant change in the dissipated power becomes evident in the thermal images and it makes it difficult to make direct, quantitative, and mutual comparisons of the thermal images, because the amplitude in the dissipated power varies from image to image. Since power is not a linear function of current, it is not possible to normalize the images and we are left to see if Joule heating changes monotonically. It must be mentioned that under white light illumination, a photoconductivity effect is observed, increasing the electrical conductivity by 3.6% in 40 min. However, under experimental conditions, red light ($\lambda = 780$ nm) was used and no photoconductivity was noted, as the electrical conductivity always decreased.

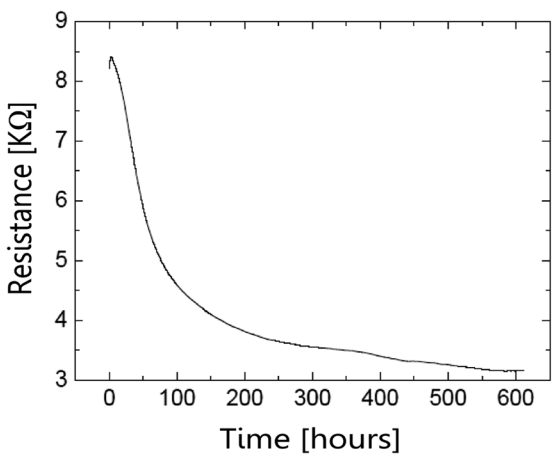

FIG. 5. Time development of the ITO nanoparticle layer in vacuum conditions. Saturation is reached in the last 50 h of the experiment.

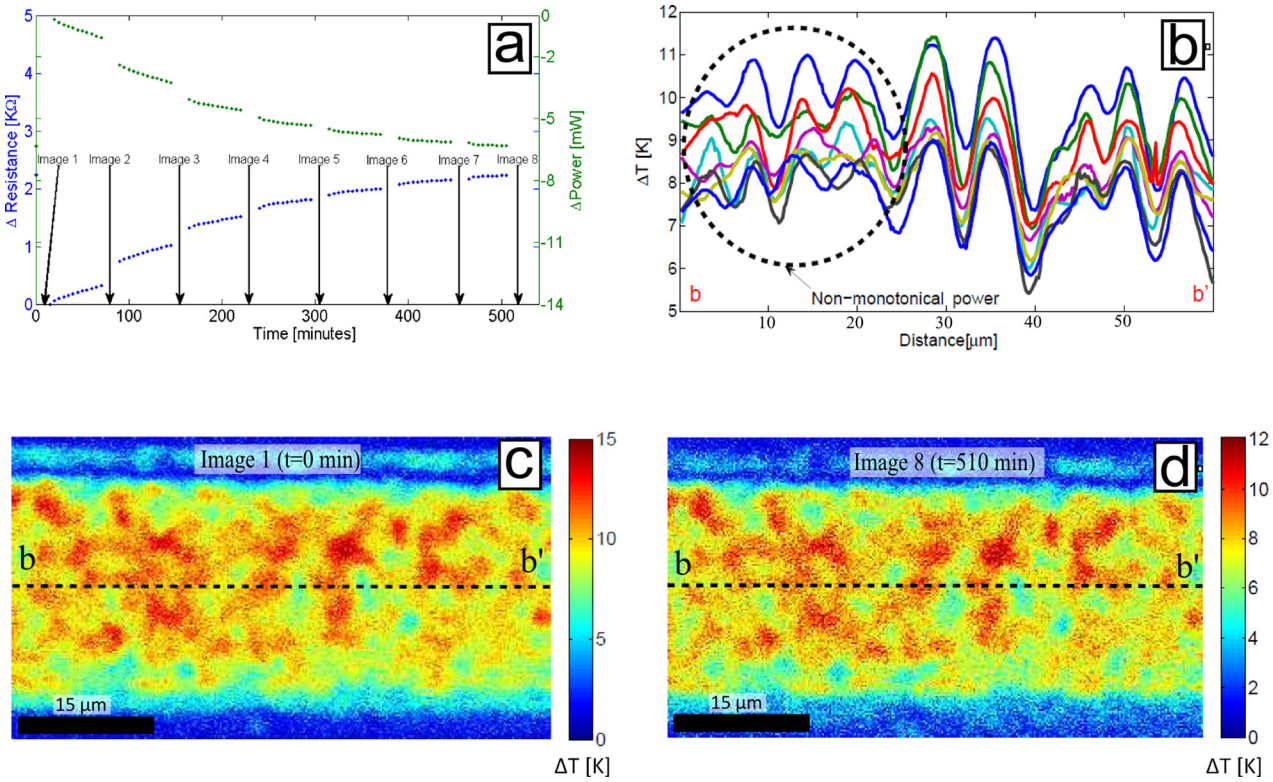

FIG. 6. (a) Time diagram showing the resistance increase in ambient conditions, its respective power decrease and the timestamps at which the thermal images were acquired. (b) Thermal profiles (for all 8 images) along the path shown in Figures 5(c) and 5(d) show non monotonic variations in temperature. Such phenomenon is attributed to the chemical reactions that occur on the surface of the oxide. (c) and (d) Comparison between the first and last thermal images show that while thermoreflectance can detect the chemically induced change conductivity in small spatial domains, at the larger scale, current conduction patterns are not affected.

In Figure 6(b), a sample profile shows that in small domains in the range of a few micrometers, the temperature or dissipated power does not decrease monotonically while in other regions it does. We can attribute the non-monotonic effects circled in Figure 6(b) to external agents that in this case correspond to the chemical reactions that occur on the surface of the oxide removing electrons from the conduction band. Figures 6(c) and 6(d) show the first and the last thermal images with adjusted color scales showing that the chemical reactions occur rather evenly on the surface and they do not considerably or visibly modify conduction paths near the surface thin film. However, we show that while the chemical reactions on the oxide surface do not considerably modify conduction patterns, at the smaller scale, they affect some domains more than others and it is possible to detect this phenomenon with thermoreflectance imaging.

CONCLUSION

We have successfully applied thermoreflectance on a highly transparent layer, and obtained the two dimensional Joule heating response in the nanoparticle thin film, showing that percolation in current paths induces strongly inhomogeneous heat loads that create thousands of "micro-hotspots" throughout the thin film. The experimental measurement is then compared to a simulation corroborating that the inhomogeneous heat loads match that of a percolative network. While percolation induced hotspots are 20% hotter than the average temperature for the given spacial resolution, we report non-Joule enhanced hotspots of a few microns that heat faster than the square of the current and show that if temperature dependent resistance is taken into account, a feedback loop between heating and resistance is formed leading to non-Joule behavior. Finally, it is shown that chemical reactions that modify the conductivity of the thin film can be detected using thermoreflectance. The resulting strongly inhomogeneous heat loads due to percolation effects could be of great interest for technologies that employ nanostructured transparent conductors since high performance TCs will most likely fall in the percolative regime,[17] and while every material may respond differently, inhomogeneous heat loads should be expected.

ACKNOWLEDGMENTS

We would like to acknowledge the California Alliance for Minority Participation Program (CAMP) and Evonik Industries AG for providing and preparing the samples.

[1]K. Y. Kim and S. B. Park, "Preparation and property control of nano-sized indium tin oxide particle," Mater. Chem. Phys. **86**(1), 210–221 (2004).
[2]A. Gutsch, H. Mühlenweg, and M. Krämer, "Tailor-made nanoparticles via gas-phase synthesis," Small **1**(1), 30–46 (2005).
[3]R. A. Gilstrap, Jr. and C. J. Summers, "Synthesis and analysis of an indium tin oxide nanoparticle dispersion," Thin Solid Films **518**(4), 1136–1139 (2009).
[4]M. Gross *et al.*, "Conductance enhancement mechanisms of printable nanoparticulate indium tin oxide (ito) layers for application in organic electronic devices," Adv. Eng. Mater. **11**(4), 295–301 (2009).

[5]G. Bühler, D. Thölmann, and C. Feldmann, "One-pot synthesis of highly conductive indium tin oxide nanocrystals," Adv. Mater. **19**, 2224–2227 (2007).
[6]J. Puetz, N. Al-Dahoudi, and M. A. Aegerter, "Processing of transparent conducting coatings made with redispersible crystalline nanoparticles," Adv. Eng. Mater. **6**(9), 733–737 (2004).
[7]M.-s. Hwang *et al*., "Inkjet-printing of indium tin oxide (ITO) films for transparent conducting electrodes," Mater. Sci. Eng., B **176**(14), 1128–1131 (2011).
[8]K. Y. Yang *et al*., "Direct indium tin oxide nanoparticle printing technique for improvement of light extraction efficiency of GaN-based LEDs," J. Electrochem. Soc. **157**(11), H1067–H1070 (2010).
[9]H. Sung-Jei, K. Yong-Hoon, and H. Jeong-In, "Development of ultrafine indium tin oxide (ito) nanoparticle for ink-jet printing by low-temperature synthetic method," IEEE Trans. Nanotechnol. **7**(2), 172–176 (2008).
[10]J. Ederth *et al*., "Thin porous indium tin oxide nanoparticle films: Effects of annealing in vacuum and air," Appl. Phys. A **81**, 1363–1368 (2005).
[11]J. Ederth *et al*., "Electrical and optical properties of thin films consisting of tin-doped oxide nanoparticles," Phys. Rev. B **68**, 155410/1-10 (2003).
[12]J. Ederth *et al*., "Electrical and optical properties of thin films prepared by spincoating a dispersion of nano-sized tin-doped indium oxide particles," Smart Mater. Struct. **11**, 675–678 (2002).
[13]G. Guenther *et al*., "Formation of metallic indium-tin phase from indium-tin-oxide nanoparticles under reducing conditions and its influence on the electrical properties," J. Appl. Phys. **104**(3), 034501 (2008).
[14]M. Gross, A. Winnacker, and P. J. Wellmann, "Electrical, optical and morphological properties of nanoparticle indium-tin-oxide layers," Thin Solid Films **515**(24), 8567–8572 (2007).
[15]R. Theissmann *et al*., "Crystallographic reorientation and nanoparticle coalescence," Phys. Rev. B **78**, 205413 (2008).
[16]Y. Zhang *et al*., "Control of catalytic reactions at the surface of a metal oxide nanowire by manipulating electron density inside it," Nano Lett. **4**, 403–407 (2004).
[17]S. De and J. N. Coleman, "The effects of percolation in nanostructured transparent conductors," MRS Bull. **36**(10), 774–781 (2011).
[18]P. M. Mayer, D. Lüerssen, R. J. Ram, and J. a Hudgings, J. Opt. Soc. Am. A **24**, 1156–1163 (2007).
[19]M. Farzaneh *et al*., "CCD-based thermoreflectance microscopy: Principles and applications," J. Phys. D: Appl. Phys. **42**, 143001 (2009).
[20]P. K. L. Chan, K. P. Pipe, G. Qin, and Z. Ma, Appl. Phys. Lett. **89**, 233521 (2006).
[21]B. Vermeersch *et al*., "Time and frequency domain CCD-based thermoreflectance techniques for high-resolution transient thermal imaging," in *26th Annual IEEE Semiconductor Thermal Measurement and Management Symposium (SEMI-THERM)* (2010), pp. 228–234.
[22]Y. K. Koh, S. L. Singer, W. Kim, J. M. O. Zide, H. Lu, D. G. Cahill, A. Majumdar *et al*., "Comparison of the 3ω method and time-domain thermoreflectance for measurements of the cross-plane thermal conductivity of epitaxial semiconductors," J. Appl. Phys. **105**(5), 054303 (2009).
[23]B. Vermeersch and A. Shakouri, "Simultaneous thermal imaging of Peltier and Joule effects," in Book of Extended Abstracts, IMAPS ATW on Thermal Management, Palo Alto, CA, 28–30 September 2010.
[24]T. Minami, "Present status of transparent conducting oxide thin-film development for indium-tin-oxide (ITO) substitutes," Thin Solid Films **516**, 5822 (2008).
[25]T. Miyata, Y. Ohtani, T. Kuboi, and T. Minami, "Stability of nano-thick transparent conducting oxide films for use in a moist environment," Thin Solid Films **516**, 1354 (2008).
[26]T. Ashida, A. Miyamura, N. Oka, Y. Sato, T. Yagi, N. Taketoshi, T. Baba, and Y. Shigesato, J. Appl. Phys. **105**, 073709 (2009).